COMPUTED TOMOGRAPHY

Intra-individual consistency of spectral detector CT-enabled iodine quantification of the vascular and renal blood pool

Simon Lennartz[1,2] · Nuran Abdullayev[1] · David Zopfs[1] · Jan Borggrefe[1] · Victor-Frederic Neuhaus[1] ·
Thorsten Persigehl[1] · Stefan Haneder[1] · Nils Große Hokamp[1]

Abstract

Objectives The objective of this study was to evaluate the intra-individual, longitudinal consistency of iodine measurements regarding the vascular and renal blood pool in patients that underwent repetitive spectral detector computed tomography (SDCT) examinations to evaluate their utility for oncologic imaging.

Methods Seventy-nine patients with two ($n = 53$) or three ($n = 26$) clinically indicated biphasic SDCT scans of the abdomen were retrospectively included. ROI-based measurements of Hounsfield unit (HU) attenuation in conventional images and iodine concentration were performed by an experienced radiologist in the following regions (two ROIs each): abdominal aorta, vena cava inferior, portal vein, and renal cortices. Modified variation coefficients (MVCs) were computed to assess intra-individual longitudinal between the different time points.

Results Variation of HU attenuation and iodine concentration measurements was significantly lower in the venous than in the arterial phase images (attenuation/iodine concentration: arterial − 4.2/− 3.9, venous 0.4/1.0; $p \le 0.05$). Regarding attenuation in conventional images of the arterial phase, the median MVC was − 1.8 (− 20.5–21.3) % within the aorta and − 6.5 (− 44.0–25.0) % within the renal cortex while in the portal venous phase, it was 0.62 (− 11.1–11.7) % and − 1.6 (− 16.2–10.6) %, respectively. Regarding iodine concentration, MVC for arterial phase was − 2.5 (− 22.9–28.4) % within the aorta and − 5.8 (− 55.9–29.6) % within the renal cortex. The referring MVCs of the portal venous phase were − 0.7 (− 17.9–16.9) % and − 2.6 (− 17.6–12.5) %.

Conclusions Intra-individual iodine quantification of the vascular and cortical renal blood pool at different time points works most accurately in venous phase images whereas measurements conducted in arterial phase images underlay greater variability.

Key Points

- *There is an intra-individual, physiological variation in iodine map measurements from dual-energy computed tomography.*
- *This variation is smaller in venous phase examinations compared with arterial phase and therefore venous phase images should be preferred to minimize this intra-individual variation.*
- *Care has to be taken, when considering iodine measurements for clinical decision-making, particularly in the context of oncologic initial or follow-up imaging.*

Keywords Contrast media · Kidney · Tomography, X-ray computed · Aorta · Vena cava, inferior

✉ Nils Große Hokamp
nils.grosse-hokamp@uk-koeln.de

1. Faculty of Medicine and University Hospital Cologne, Department of Diagnostic and Interventional Radiology, University of Cologne, Kerpener Str. 62, 50937 Cologne, Germany

2. Else Kröner Forschungskolleg Clonal Evolution in Cancer, University Hospital Cologne, Weyertal 115b, 50931 Cologne, Germany

Abbreviations

ANOVA	Analysis of variances
AP	Anterior-posterior
CI	Conventional images
CT	Computed tomography
CTDIvol	Volumetric computed tomography dose index
D_E	Effective diameter
DECT	Dual-energy computed tomography
HU	Hounsfield units
IC	Iodine concentration

ICC   Intraclass correlation coefficient
IM   Iodine maps
LAT   Lateral
MVC   Modified variation coefficient
RADS   Reporting and data storage system
RECIST   Response evaluation criteria in solid tumors
RIS   Radiological information system
ROI   Region of interest
SDCT   Spectral detector computed tomography

Introduction

Oncologic imaging and tumor response assessment rely on standardized image acquisition warranting reproducible data. In the past, various imaging criteria frameworks were established for the purpose of accurate diagnosis and follow-up imaging of oncologic diseases in a structured fashion (e.g., RECIST, Li-RADS, and Lung-RADS) [1–3]. As patient-tailored regimes including novel approaches such as targeted therapy or immune checkpoint inhibition continuously gained importance, some of these frameworks had to be adapted in order to pursue best possible image-guided follow-up (e.g., iRECIST) [4]. For both, initial diagnosis and follow-up, tumor vascularization represents a key criterion, for example applied in hepatocellular carcinoma [3]. Therefore, in computed tomography (CT), iodinated contrast media are widely used to facilitate detailed characterization of tissue and/or lesion vascularization in multiphasic examinations. However, in conventional CT, Hounsfield units (HU) of a given voxel not only solely reflect the amount of circulating iodinated contrast media but also the underlying tissue or superposing artifacts.

Over the past years, dual-energy computed tomography (DECT) systems have been shown to enable material separation based on separate acquisition of attenuation characteristics of two energy spectra. This has led to the development of material-specific reconstructions such as iodine maps. Clinically, these iodine maps have been investigated with regard to their diagnostic value in assessing various malignant diseases of the abdomen such as hepatocellular carcinoma [5, 6], renal cell carcinoma [7, 8], and pancreatic cancer [9, 10]. Besides the improvement of subjective delineation and detection of malignant lesions, accurate quantification of iodine and its evaluation as a potential imaging biomarker has been in the focus of scientific interest. Hence, the accuracy with which such DECT-derived iodine quantification can be conducted has been subject to previous investigations: in recent phantom studies, it was shown that iodine can be accurately quantified with latest generation DECT scanners, although in some of them, it was reported that measurement errors differ between

vendors and phantom sizes [11–13]. As one of the tested DECT systems, the so-called spectral detector CT (SDCT), at which the two energy spectra are registered on the detector level, was reported to yield accurate iodine quantification even in low measurement ranges [11, 14].

Although potential oncologic applications of iodine quantification have been frequently examined, little is known about intra-individual reproducibility of these measurements in vivo resulting in a crucial need for systematic in vivo evaluation of this matter. In a previous study, it was shown that the iodine quantity within portal vein, liver parenchyma, and liver lesions varied significantly between repetitive scans. Although these results were of interest, at least a part of the inter-scan variability may originate from the dual hepatic blood supply implying regulation of hepatic perfusion by various fluctuating physiological determinants [15]. By contrast, the peritubular capillary perfusion of the renal cortex is rather consistent as it is highly autoregulated [16].

Hence, the rationale of this study was to assess the method-inherent, intra-individual variability of SDCT-derived iodine quantification in large abdominal vessels and the renal cortex as a reference region with relatively low perfusion variability. Hereby, we aimed to investigate the suitability of iodine quantification as a quantitative imaging biomarker for oncologic follow-up.

Materials and methods

Study population

After informed patient consent was waived by the local institutional review board, a structured query to the radiological information system (RIS) was carried out to identify all patients who received ≥ 2 SDCT scans of the abdomen between May 2016 and December 2017. Out of these patients, we identified 79 eligible patients of which 26 underwent biphasic abdominal SDCT thrice and 53 twice. Exclusion criteria were a modified scan protocol in order to reduce contrast media, age ≤ 18 years and renal artery stenosis. The detailed workflow for study inclusion is given in Fig. 1. All patients exhibited a glomerular filtration rate ≥ 30 ml/min. Reasons for examination comprised oncologic staging for melanoma ($n = 55$), sarcoma ($n = 12$), lung ($n = 8$), or GI-tumors ($n = 4$). Imaging examinations were reviewed for the presence of new ascites or pleural effusion. A significant change in body weight was excluded based on computation of the effective diameter (D_E). Anterior-posterior (AP) and lateral (LAT) diameter were determined using an automated script within the Matlab environment (MathWorks) and D_E was determined using the formula $D_E = \sqrt{AP \, x \, LAT}$ [17].

Fig. 1 Flow chart for study inclusion. We included 53 patients who underwent double examinations and 26 patients who received triple scans resulting in 184 scans in total

Database query to PACS/RIS for patients who underwent two or three biphasic Spectral Detector CT scans of the abdomen
n = 94

Monophasic scan, n = 4

Reduced contrast media dose or unenhanced scan, n = 9

Incomplete image acquisition, n = 2

n = 79 patients (n = 184 scans) eligible for study inclusion

n = 53 patients who received double scans (n = 106 scans)

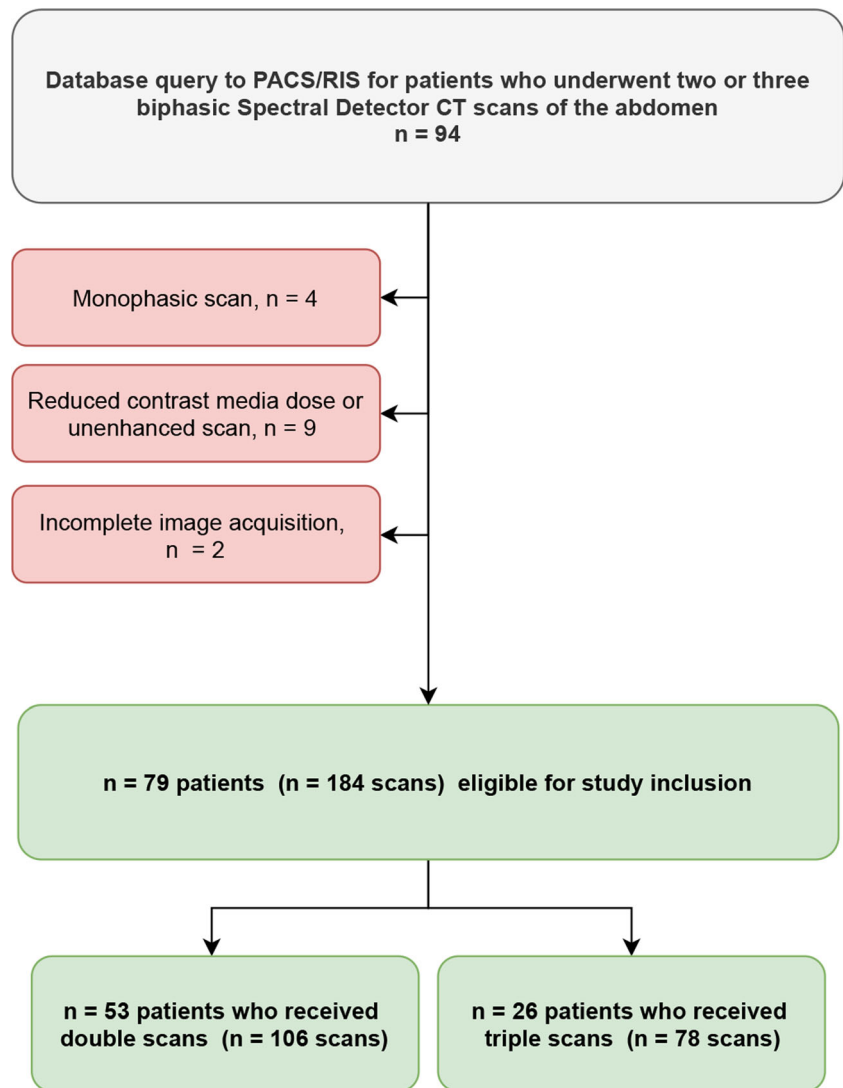n = 26 patients who received triple scans (n = 78 scans)

## Image acquisition, reconstruction, and post-processing

All acquired scans were clinically indicated and conducted on a SDCT system (IQon, Philips Healthcare). As it is comprised within the routine imaging protocol, a bolus of iodinated contrast agent (Accupaque 350 mg/ml, GE Healthcare) was applied intravenously followed by a 30-ml saline chaser at a flow rate of 3.5 ml/s using a 20-G catheter. Scans were conducted 16 and 50 s after a threshold of 150 HU in an ROI placed in the descending aorta just below the diaphragm was reached to acquire arterial and portal venous phase images, respectively. Between the repetitive scans, patient positioning, contrast media injection, and image acquisition were performed consistently. Image acquisition parameters were the following: enabled dose modulation (DoseRight 3D-DOM, Philips Healthcare), collimation 64 × 0.625 mm, rotation time 0.33 s, pitch 0.671, tube voltage 120 kVp, and matrix 512 × 512. Conventional images (CIs)

and iodine maps (IM) were reconstructed with a spectral image reconstruction algorithm (Spectral, filter B, denoising level 3, Philips Healthcare) in the axial plane (Fig. 2), with a slice thickness and section increment of 2 mm. The CIs reconstructed with this algorithm have been shown to be identical to images reconstructed with the vendor's hybrid-iterative reconstruction algorithm [18].

Image analysis

To acquire Hounsfield unit (HU) attenuation from CI and iodine concentration (IC) from IM, a radiologist with 5 years of experience in abdominal imaging placed two circular regions of interest (ROI) in each of the following localizations: left and right renal cortex, aorta, portal vein, and inferior vena cava (electronic supplement 1 illustrates ROI placement). In a subgroup of randomly chosen 30 examinations, ROIs were placed in supra- and infrarenal segment of the abdominal aorta

Fig. 2 SDCT-derived conventional image and quantitative iodine map of the portal venous phase showing both kidneys in the coronal plane

Conventional image

Quantitative iodine map
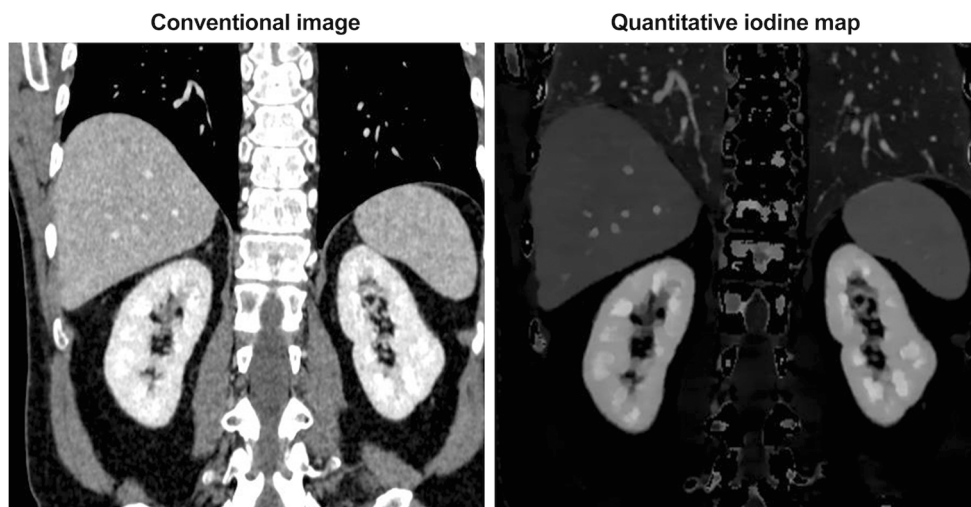
to determine significant differences. In the same subset, ROIs were placed by a second reader to assess inter-reader reliability. ROI placement took place within the vendor's proprietary image viewer (IntelliSpace Portal 9, Philips Healthcare). ROIs were drawn in order to cover the largest possible area of the vessel or renal cortex but to exclude irrelevant circumjacent tissue. All consecutive scans of one patient were reviewed after another to facilitate consistent intra-individual ROI placement. To evaluate longitudinal variability of HU and IC, as suggested before, we used a modified variation coefficient (MVC) representing the difference between two consecutive scans relatively to the percental mean between these two scans [15, 19]:

$$ MVC = \frac{(x_{i+1} - x_i)}{(x_{i+1} + x_i) \times 0.5} \times 100\% $$

As suggested earlier [15], organ measurements were normalized to the abdominal aorta to account for intra-individual perfusion differences; normalized values were obtained by division of the measured concentration by the concentration within the abdominal aorta.

Confounder analysis

To determine whether the gradient of the contrast medium filing during the bolus tracking period had any effect on the quantitative measurements of HU and IC, the bolus tracking graph curves of every scan were analyzed by calculating the slope of the bolus tracking graph from its start to the crossing point with the 150 HU threshold line (Fig. 3). The differences between the slopes of repetitive scans (Δslope) were calculated and the degree of correlation between Δslope and the modified variation coefficients of the referring scans was determined.

Statistical analysis

Statistical assessments were performed with JMP (v13, SAS Institute). Bivariate Pearson correlation was used to analyze the influence of the speed of arterial contrast media filling during the bolus tracking period on the modified variation coefficients between the referring scans. Inter-reader reliability was determined by computation of the intraclass correlation coefficient as suggested earlier [20]. Two-way analysis of variances (ANOVA) was used to compare MVCs. Statistical significance was defined as $p \leq 0.05$. Modified variation coefficients, as well as absolute attenuation and iodine measurements, are reported as median and 10/90% quantile.

Results

Patients

The overall time between examinations was 167 ± 85 days. In patients with double examinations, the mean inter-scan period was 185 ± 93 days and in patients with triple examinations, it was 145 ± 65 days between the first and the second scan and 146 ± 69 days between the second and the third scan. CTDIvol in patient examinations was 13.48 ± 5.99 mGy. Average D_E was 29.95 cm. Intra-individual average change in D_E was -1%, while the greatest difference was $+8\%$ only. No significant difference in D_E was found between the initial and follow-up groups ($p \leq 0.05$). No new ascites and/or pleural effusion was found.

General variability

In arterial phase images, median attenuations acquired from conventional images were 324.3 (236.6–424.9) HU (aorta) and 177.3 (117.3–233.2) HU (renal cortex) and the corresponding iodine concentrations were 11.9 (8.0–16.1) mg/ml
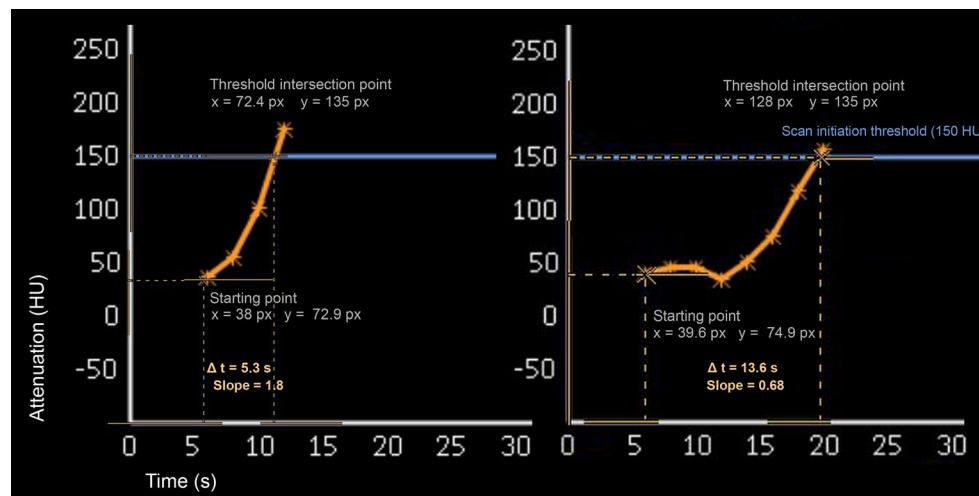
Fig. 3 Tracker graph analysis of two CT scans with fast (left) and slow (right) contrast media influx. Starting and threshold intersection points were determined to calculate the slope of the tracker graph in order to evaluate the gradient and speed of contrast media influx as a possible confounder with regard to the iodine and HU measurements

and 5.7 (3.5–7.9) mg/ml. In portal venous phase images, mean attenuations were 157.3 (123.6–198.1) HU (aorta), 180.8 (141.7–226.0) HU (renal cortex), 165.7 (127.4–211.1) HU (portal vein), and 111.4 (77.9–137.7) (inferior vena cava) and the iodine concentrations were 4.7 (3.3–6.7) (aorta), 6.0 (4.1–7.8) (renal cortex), 5.2 (3.7–7.4) (portal vein), and 3.0 (1.5–4.2) (inferior vena cava). The distribution of absolute attenuation and iodine concentration values for the different ROIs is illustrated in Fig. 4. For the subgroup in which supra- und infrarenal portion of the abdominal aorta was assessed separately, a close correlation without significant differences was found ($R^2 = 0.892$–0.976; $p = 0.40$–0.91).

Intra-individual variability

Averaged over all ROIs, intra-individual longitudinal consistency was on a comparable level in iodine and attenuation measurements ($p = 0.27$). The overall median MVC was -0.37 (-21.0–17.1) % and -1.6 (-28.4–23.4) % for attenuation and iodine concentration, respectively (Table 1). Averaged over all ROIs, median MVCs of attenuation ($\text{MVC}_\text{arterial}$, -4.2 (-32.5–22.6) %; MVC_venous, 0.4 (-14.7–15.4) %) and iodine concentration ($\text{MVC}_\text{arterial}$, -3.9 (-37.8–29.2) %; MVC_venous, 1.0 (-21.7–21.5) %) were significantly lower in portal venous than in arterial phase images (both $p \leq 0.05$; Fig. 5).

Regarding attenuation in conventional images of the arterial phase, the median MVC_HU was -1.8 (-20.5–21.3) % (aorta) and -6.5 (-44.0–25.0) % (renal cortex). For portal venous phase images, MVC_HU was 0.6 (-11.1–11.7) % (aorta), -2.0 (-16.2–10.6) % (renal cortex), 2.4 (-10.3–15.8) % (portal vein), and -0.0 (-22.8–29.5) % (inferior vena cava).

Pertaining to the iodine concentration measurements, MVC_IC for arterial phase was -2.5 (-22.9–28.4) % (aorta) and -5.8 (-55.9–29.6) % (renal cortex) while it was -0.7 (-17.9–16.9) % (aorta), -2.6 (-17.6–12.5) % (renal cortex), 0.9 (-18.0–20.8) % (portal vein), and -2.3% (-40.8–40.8) (inferior vena cava) for portal venous phase images, respectively. Figure 6 demonstrates the MVC of iodine concentration and Hounsfield unit attenuation in ROI-specific waterfall plots.

Normalization of the renal cortex to the aorta did not have a significant effect on the variability for either iodine ($p = 0.69$–0.74) or attenuation measurements, although there was a trend towards lower variability in arterial phase images when normalization was conducted: pertaining to iodine measurements, normalized MVC_IC of the renal cortex was 3.2 (-48.3–22.5) % (arterial phase) and -1.9 (-18.6–16.3) % (portal venous phase) while for HU attenuation, it was -0.9 (-36.2–18.5) % (arterial phase) and -2.3 (-15.1–10.5) % (portal venous phase).

Confounder analysis

Regarding the confounder analysis, we found that the difference in arterial contrast media filling speed represented by the difference between the slopes of the bolus tracking graphs of repetitive scans (Δslope) exhibited a random correlation to the MVCs of the attenuation and iodine concentration measurements ($R^2_\text{HU} = 0.00$–0.05; $R^2_\text{Iodine} = 0.00$–0.06; $p > 0.05$). Inter-reader agreement was excellent for both venous and arterial phase (ICC > 0.8).

Discussion

Iodine quantification enabled by DECT is a feasible tool to precisely determine contrast media distribution and can be considered as an imaging surrogate parameter for organ/lesion perfusion [21]. In the past, it was proven to be useful with regard to detection [22, 23], classification [7, 24–29], and
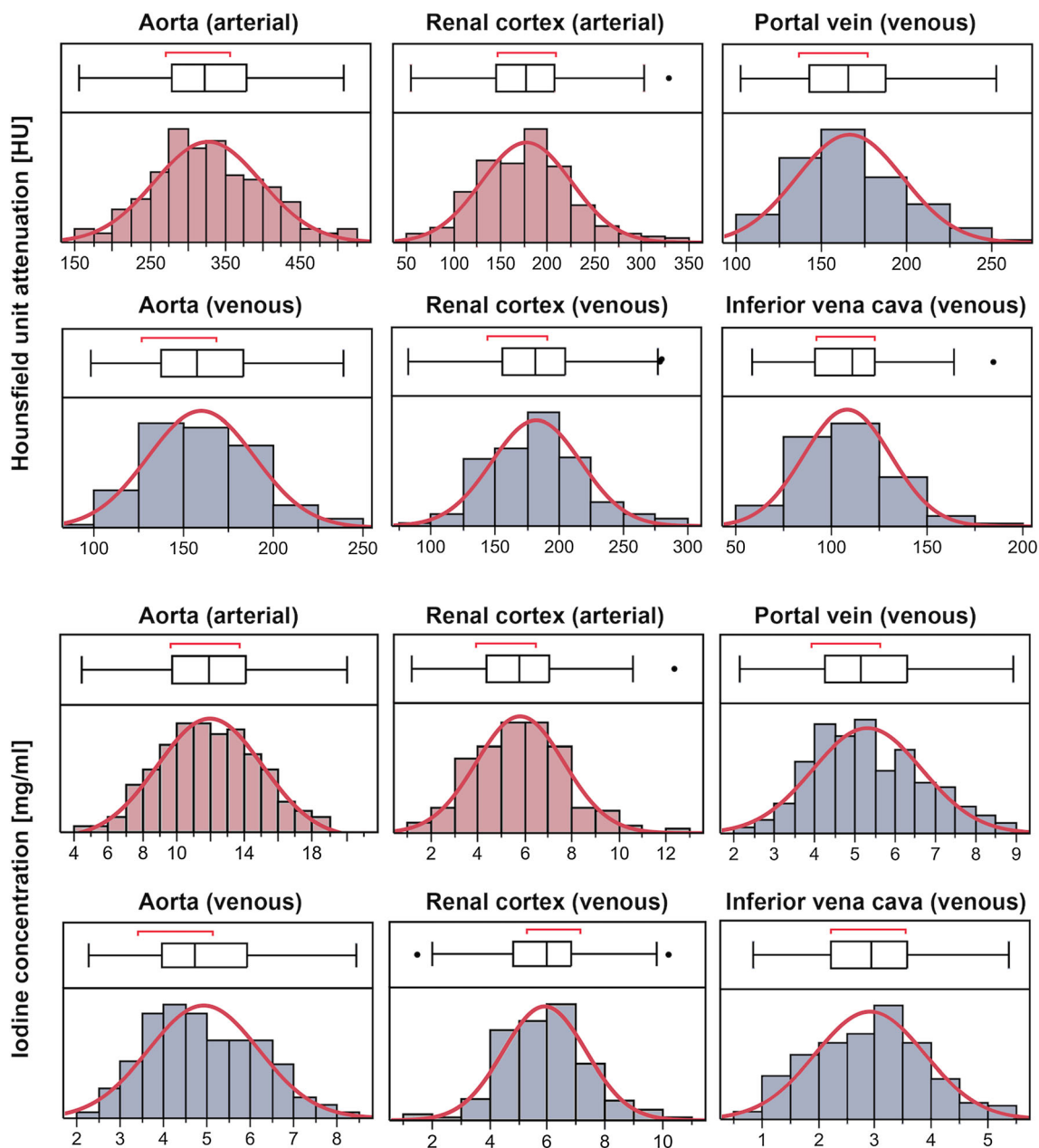
Fig. 4 Distribution of absolute values of Hounsfield unit (HU) attenuation and iodine concentration (mg/ml) within the different ROIs (aorta, renal cortex, portal vein, inferior vena cava)

response assessment [30–33] of various malignant diseases. Recent studies suggest that iodine quantification performed on the latest generation DECT systems works with high precision [11, 12]. However, especially when being applied to response assessment or follow-up imaging, DECT-enabled iodine measurements should also warrant a high level of intra-individual reproducibility. Still, the current base of evidence regarding this issue is insufficient.

In this study, we examined the longitudinal intra-individual consistency of iodine quantification in vivo and focused on the vascular and renal cortical blood pool. As opposed to other parenchymal organs, e.g., the liver, whose dual blood supply entails multifaceted physiological influences on organ perfusion, the renal cortical blood pool primarily reflects the glomerular and peritubular capillary bed. As its perfusion is highly autoregulated to maintain a consistent organ function [16], the renal cortex is predestined to test the longitudinal consistency of organ parenchymal iodine quantification while excluding physiological influences that could account for variability as far as possible. As vascular regions of interest, the abdominal aorta, the portal vein, and the vena cava inferior were chosen to reflect the pre- and post-capillary blood pool.

We found that longitudinal differences between repetitive examinations were significantly higher in arterial phase

Table 1 Mean variation coefficient of attenuation and iodine concentration in arterial and venous phase

	Region of interest		Mean variation coefficient			
			Mean ± SD (%)	10% quantile (%)	Median (%)	90% quantile (%)
Attenuation	Arterial	Aorta	− 0.7 ± 18.0	− 20.5	− 1.8	21.3
		Kidney	− 7.0 ± 27.7	− 44.0	− 6.5	25.0
	Venous	Aorta	0.3 ± 9.9	− 11.1	0.6	11.7
		Kidney	− 2.5 ± 13.8	− 16.2	− 1.6	10.6
		Portal vein	2.5 ± 13.9	− 10.3	2.4	15.8
		Inferior vena cava	0.8 ± 18.7	− 22.8	− 0.0	29.5
Iodine concentration	Arterial	Aorta	− 0.7 ± 22.5	− 22.9	− 2.5	28.4
		Kidney	− 7.9 ± 33.1	− 55.9	− 5.8	29.6
	Venous	Aorta	− 0.7 ± 15.0	− 17.9	− 0.7	16.9
		Kidney	− 2.7 ± 20.7	− 17.6	− 2.6	12.5
		Portal vein	2.5 ± 20.2	− 18.0	0.9	20.8
		Inferior vena cava	− 1.1 ± 30.6	− 40.8	− 2.3	40.8

images for both attenuation and iodine concentration, whereas in portal venous phase images, the modified variation coefficient of 80% of the patients was within a range of ± 15% regarding all ROIs except for the vena cava inferior which revealed a much higher variability. Considering the reported high precision of iodine quantification, the usage of a consistent protocol for image acquisition/reconstruction as well as contrast media administration, and the blood supply characteristics of the renal cortex described earlier, this variability can be assumed to result mainly from fluctuating cardiovascular determinants. As functional cardiac parameters were not available for our study cohort, we considered the influence of the speed of aortic contrast media filling during the bolus

tracking period as a surrogate parameter that at least partially reflects the cardiac output; however, no correlation was found.

A recent study reported the variability for iodine measurements of the liver parenchyma not to exceed 20% in 80% of the patients [15]. Compared with these results, the renal cortical variability regarding iodine measurements in the portal venous phase found in our study was smaller with around 15%. This may be explained by the different vascular supply characteristics of the two organs alluded to earlier.

The significantly lower intra-individual variability in portal venous phase measurements compared with the arterial phase is likely due to its longer scan delay. Therefore, volatile physiological factors on the vascular and parenchymal blood pool
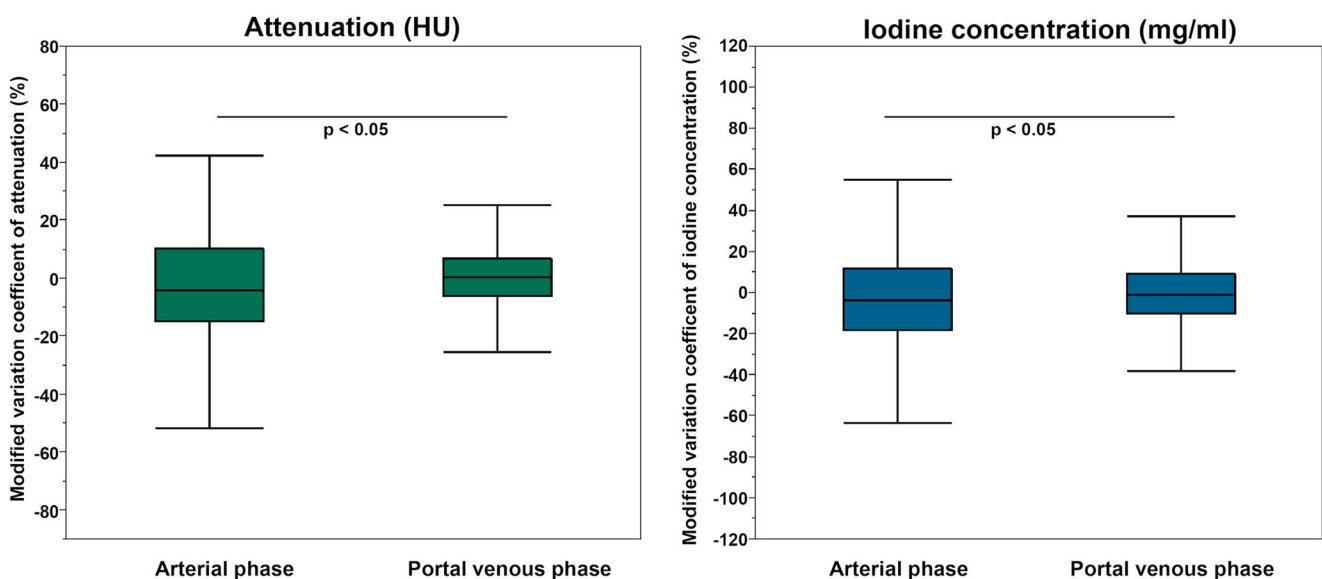

Fig. 5 Distribution of absolute values of Hounsfield unit (HU) attenuation and iodine concentration (mg/ml) within the different ROIs (aorta, renal cortex, portal vein, inferior vena cava)
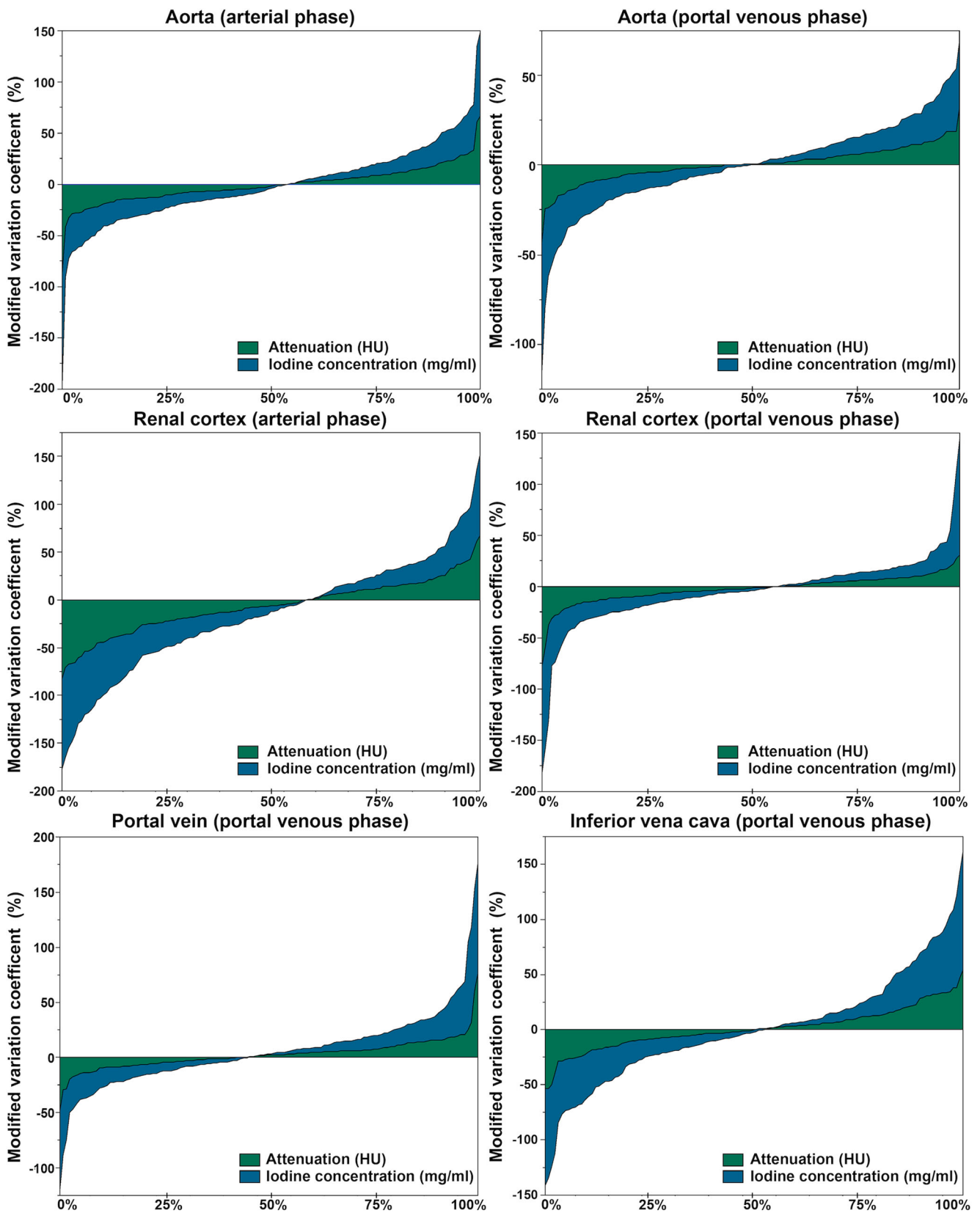
Fig. 6 Waterfall plots illustrating the modified variation coefficients regarding Hounsfield unit attenuation (green) and iodine concentration (blue)

may be equilibrated to some extent resulting in a higher level of longitudinal reproducibility. Previous studies comparing DECT-derived iodine quantification to perfusion CT reported an optimal correlation between the two at a scan delay of 15–21 s [34] and 9 s [5] for imaging of the pancreas and liver, respectively. Taking these results and the higher variability we found in arterial phase images into account, it becomes obvious that when determining the optimal scan delay for organ-specific monophasic snapshot iodine quantification, a certain trade-off between best possible accuracy and reproducibility might be necessary. Yet, when performing measurements of iodine concentration, this physiologic variability needs to be considered for evaluation, especially in the context of oncologic imaging.

Apart from its retrospective nature, there are limitations to our study that need to be discussed. First, we only included the renal cortex as a representative parameter for organ parenchyma although, in the light of the abovementioned considerations, an organ-specific analysis of longitudinal variation seems reasonable; this approach was substantiated on our premise to minimize physiological regulation factors as far as possible. In addition, the iodine concentration found in the renal cortex may be higher than in some tumors. Second, as alluded earlier, we did not consider functional cardiac parameters as they were not available for our study cohort. The number of patients included in this study is limited. We automatically determined the water equivalent diameter to be indicative of body weight; however, the body mass index might be a more appropriate parameter but could not be calculated for all patients. Last, the results provided in this study only apply for the SDCT system and the acquisition and reconstruction procedure we chose.

Conclusively, this study shows that SDCT-enabled iodine quantification of the renal blood pool in portal venous phase images is subject to a longitudinal variability of approximately 15% while in arterial phase images, this variability is significantly higher. Thus, when applying iodine measurements in the abdomen, e.g., for oncologic follow-up, this variability should be considered. Moreover, when calculating quantitative iodine thresholds, venous phase images should be preferred while particular care has to be taken when using arterial phase images.

Compliance with ethical standards

Guarantor The scientific guarantor of this publication is Dr. Nils Große Hokamp.

Conflict of interest SL received research and travel support outside this specific project from Philips Healthcare. JB, DM received speaker's honoraria from Philips Healthcare. NGH received speaker's honoraria and travel support from Philips Healthcare. All other authors: nothing to disclose.

Statistics and biometry No complex statistical methods were necessary for this paper.

Informed consent Written informed consent was waived by the Institutional Review Board.

Ethical approval Institutional Review Board approval was obtained.

Methodology
• Retrospective
• Observational
• Performed at one institution

References

1. Eisenhauer EA, Therasse P, Bogaerts J et al (2009) New response evaluation criteria in solid tumours: revised RECIST guideline (version 1.1). Eur J Cancer 45(2):228–247
2. Chung K, Jacobs C, Scholten ET et al (2017) Lung-RADS category 4X: does it improve prediction of malignancy in subsolid nodules? Radiology 284(1):264–271
3. Schima W, Heiken J (2018) LI-RADS v2017 for liver nodules: how we read and report. Cancer Imaging 18
4. Seymour L, Bogaerts J, Perrone A et al (2017) iRECIST: guidelines for response criteria for use in trials testing immunotherapeutics. Lancet Oncol 18(3):e143–e152
5. Gordic S, Puippe GD, Krauss B et al (2016) Correlation between dual-energy and perfusion CT in patients with hepatocellular carcinoma. Radiology 280(1):78–87
6. Yang C-B, Zhang S, Jia Y-J et al (2017) Dual energy spectral CT imaging for the evaluation of small hepatocellular carcinoma microvascular invasion. Eur J Radiol 95:222–227
7. Mileto A, Marin D, Alfaro-Cordoba M et al (2014) Iodine quantification to distinguish clear cell from papillary renal cell carcinoma at dual-energy multidetector CT: a multireader diagnostic performance study. Radiology 273(3):813–820
8. Graser A, Becker CR, Staehler M et al (2010) Single-phase dual-energy CT allows for characterization of renal masses as benign or malignant. Invest Radiol 45(7):399–405
9. Kawamoto S, Fuld MK, Laheru D, Huang P, Fishman EK (2018) Assessment of iodine uptake by pancreatic cancer following chemotherapy using dual-energy CT. Abdom Radiol (NY) 43(2):445–456
10. Noda Y, Goshima S, Miyoshi T et al (2018) Assessing chemotherapeutic response in pancreatic ductal adenocarcinoma: histogram analysis of iodine concentration and CT number in single-source dual-energy CT. AJR Am J Roentgenol. https://doi.org/10.2214/AJR.18.19791
11. Pelgrim GJ, van Hamersvelt RW, Willemink MJ et al (2017) Accuracy of iodine quantification using dual energy CT in latest generation dual source and dual layer CT. Eur Radiol 27(9):3904–3912
12. Jacobsen MC, Schellingerhout D, Wood CA et al (2018) Intermanufacturer comparison of dual-energy CT iodine quantification and monochromatic attenuation: a phantom study. Radiology 287(1):224–234
13. Sauter AP, Kopp FK, Münzel D et al (2018) Accuracy of iodine quantification in dual-layer spectral CT: influence of iterative reconstruction, patient habitus and tube parameters. Eur J Radiol 102:83–88

14. Hua C-H, Shapira N, Merchant TE, Klahr P, Yagil Y (2018) Accuracy of electron density, effective atomic number, and iodine concentration determination with a dual-layer dual-energy computed tomography system. Med Phys 45(6):2486–2497

15. Große Hokamp N, Abdullayev N, Persigehl T et al (2018) Precision and reliability of liver iodine quantification from spectral detector CT: evidence from phantom and patient data. Eur Radiol. https://doi.org/10.1007/s00330-018-5744-0

16. Carlström M, Wilcox CS, Arendshorst WJ (2015) Renal autoregulation in health and disease. Physiol Rev 95(2):405–511

17. Boone JM, Strauss KJ, Cody DD et al American Association of Physicists in Medicine (AAPM). Size-specific dose estimates (SSDE) in pediatric and adult body CT examinations: report of AAPM Task Group 204. Available via: https://www.aapm.org/pubs/reports/RPT_204.pdf. Accessed 24 Apr 2019

18. Große Hokamp N, Höink AJ, Doerner J et al (2018) Assessment of arterially hyper-enhancing liver lesions using virtual monoenergetic images from spectral detector CT: phantom and patient experience. Abdom Radiol (NY) 43(8):2066–2074

19. Reed GF, Lynn F, Meade BD (2002) Use of coefficient of variation in assessing variability of quantitative assays. Clin Diagn Lab Immunol 9(6):1235–1239

20. Fleiss JL, Cohen J (2016) The equivalence of weighted kappa and the intraclass correlation coefficient as measures of reliability. Educ Psychol Meas 33(3):613–619

21. Thaiss WM, Haberland U, Kaufmann S et al (2016) Iodine concentration as a perfusion surrogate marker in oncology: further elucidation of the underlying mechanisms using volume perfusion CT with 80 kVp. Eur Radiol 26(9):2929–2936

22. Uhrig M, Simons D, Bonekamp D, Schlemmer H-P (2017) Improved detection of melanoma metastases by iodine maps from dual energy CT. Eur J Radiol 90:27–33

23. Muenzel D, Lo GC, Yu HS et al (2017) Material density iodine images in dual-energy CT: detection and characterization of hypervascular liver lesions compared to magnetic resonance imaging. Eur J Radiol 95:300–306

24. Altenbernd J, Wetter A, Umutlu L et al (2016) Dual-energy computed tomography for evaluation of pulmonary nodules with emphasis on metastatic lesions. Acta Radiol 57(4):437–443

25. Iwano S, Ito R, Umakoshi H, Ito S, Naganawa S (2015) Evaluation of lung cancer by enhanced dual-energy CT: association between three-dimensional iodine concentration and tumour differentiation. Br J Radiol 88(1055)

26. Rizzo S, Radice D, Femia M et al (2018) Metastatic and non-metastatic lymph nodes: quantification and different distribution of iodine uptake assessed by dual-energy CT. Eur Radiol 28(2):760–769

27. Große Hokamp N, Gupta A, Gilkeson RC (2019) Stratification of pulmonary nodules using quantitative iodine maps from dual-energy computed tomography. Am J Respir Crit Care Med 199(2):e3–e4

28. Borggrefe J, Neuhaus V-F, Le Blanc M et al (2018) Accuracy of iodine density thresholds for the separation of vertebral bone metastases from healthy-appearing trabecular bone in spectral detector computed tomography. Eur Radiol. https://doi.org/10.1007/s00330-018-5843-y

29. Lennartz S, Le Blanc M, Zopfs D et al (2019) Dual-energy CT-derived iodine maps: use in assessing pleural carcinomatosis. Radiology. https://doi.org/10.1148/radiol.2018181567

30. Uhrig M, Simons D, Ganten M-K, Hassel JC, Schlemmer H-P (2015) Histogram analysis of iodine maps from dual energy computed tomography for monitoring targeted therapy of melanoma patients. Future Oncol 11(4):591–606

31. Baxa J, Matouskova T, Krakorova G et al (2016) Dual-phase dual-energy CT in patients treated with erlotinib for advanced non-small cell lung cancer: possible benefits of iodine quantification in response assessment. Eur Radiol 26(8):2828–2836

32. Hellbach K, Sterzik A, Sommer W et al (2017) Dual energy CT allows for improved characterization of response to antiangiogenic treatment in patients with metastatic renal cell cancer. Eur Radiol 27(6):2532–2537

33. Bargellini I, Crocetti L, Turini FM et al (2018) Response assessment by volumetric iodine uptake measurement: preliminary experience in patients with intermediate-advanced hepatocellular carcinoma treated with Yttrium-90 radioembolization. Cardiovasc Intervent Radiol 41(9):1373–1383

34. Skornitzke S, Fritz F, Mayer P et al (2018) Dual-energy CT iodine maps as an alternative quantitative imaging biomarker to abdominal CT perfusion: determination of appropriate trigger delays for acquisition using bolus tracking. Br J Radiol 91(1085):20170351